



41

42 **ABSTRACT**

43 In this paper, we present a ROad SEgment-based emission model (ROSE) for transportation Green House Gas  
44 (GHG) emissions estimation. The objective of this study is to provide a framework for quickly estimating  
45 traffic-related GHG emissions and analyzing its spatiotemporal distribution and variation based on real-time  
46 traffic data. The model has carried out a combination of Intelligent Transport System (ITS) technology,  
47 Geographic Information System (GIS) technology, and the International Vehicle Emission Model (IVE). In the  
48 ROSE model, the ITS' floating car data (FCD) and loop detector data (LDD) are used as the model input. The IVE  
49 model is used for providing microscopic vehicle emission rates; and GIS is not only used as a database exchanger,  
50 but also used as a computation and a visualization tool in the ROSE model. This paper will discuss two  
51 fundamental works conducted in our ROSE model research project: 1) ITS real-time traffic data collection and  
52 geographic-related data unification; and 2) vehicle driving activity generation and road-segment based CO<sub>2</sub>  
53 emission computation. To demonstrate the effectiveness of the ROSE model, we apply this model in a case study  
54 for estimating the daily CO<sub>2</sub> emissions generated from the highway transportation of Beijing, China during the  
55 year 2008. The result shows that the ROSE model can provide micro-level, highly accurate, and real-time GHG  
56 emission for the whole urban area (such as Beijing city).

57

58 **1 INTRODUCTION**

59 Global climate change-induced problems have become major critical threats to life on Earth. Greenhouse Gas  
60 (GHG) emission has been considered as one of the key contributors to the threats. Reducing GHG emissions and  
61 keeping the anthropogenic CO<sub>2</sub> emission rate at a reasonable level is a great challenge. In recent years, CO<sub>2</sub>  
62 emissions from the transportation sector have been given significant attention (IPCC, 2007). It has been estimated  
63 that 23% of the world, 25% of the European, or 33% of the United States total anthropogenic CO<sub>2</sub> emissions is  
64 from the transportation sector. Road transportation currently accounts for 74% of total transport CO<sub>2</sub> emissions  
65 (IPCC, 2007; Ribeiro et al, 2007; Davis et al., 2005). With the remarkable development of urban economy and  
66 expansion of population, the CO<sub>2</sub> emissions from road transportation continue to rise.

67 Accurate quantitative measurement of urban road traffic CO<sub>2</sub> daily emission is critical in making  
68 effective policy to control transportation related CO<sub>2</sub> emissions (Carmichael et al., 2008; Escobedo et al., 2008;  
69 Barth et al., 2008). Currently, a considerable amount of on-road vehicle emission models have been developed to  
70 estimate and predict the transportation GHG emissions, at macroscopic, mesoscopic and microscopic levels  
71 (Sharma et al., 2001; Rakha et al., 2003; Abo-Qudais et al., 2005). However, when applying such models in the  
72 real world, one of the sources of model uncertainties is input information (Borrego et al., 2003). For each model,  
73 there are many parameters (e.g., vehicle engine technology conditions, vehicle starting and running activities,  
74 road conditions, weather conditions, et al.) (Barth et al., 1996) that need to provide corresponding proper  
75 experimental data.

76 The International Vehicle Emission (IVE) (Davis et al., 2005), described as an improved estimation tool for  
77 mobile source emissions, is specifically designed to improve the flexibility needed by most developing countries  
78 to address mobile source air emissions, including a large range of criteria pollutants, GHGs, and toxic emissions  
79 (Lents et al., 2004; Davis et al., 2004; Liu et al., 2005; Wang et al., 2006; Liu et al., 2007). Compared to other  
80 model-based emission models, the IVE model obtains high precision on emissions modeling while reducing some  
81 unnecessary input information. However, like the other models, one difficulty when applying the IVE model to  
82 GHG estimation is to obtain detailed and accurate data about vehicle activities. Two main approaches are used to  
83 deal with this problem. One approach is to directly input the invested traffic activity data into the IVE emission  
84 models. The other approach is to integrate the emission models with the dynamic traffic simulation model.

85 For the first approach, most research is designed to only collect representative traffic information at specific  
86 time periods and places (Liu et al., 2007). Currently, the solution is to use statistical tools to derive vehicle driving  
87 patterns from sample data and then extrapolate to cover the entire urban area. However, the results are static and  
88 cannot vary with sudden changes in traffic conditions since the investigation is subject to limited investigation  
89 locations and time periods. Moreover, extrapolating the sampling statistical results to represent the total urban area  
90 may introduce uncertainties. In addition, this investigative approach requires a large amount of manpower,  
91 material, and financial resources while the efficiency of the operations is relatively low. The dynamic traffic  
92 simulation approach can provide the time dependent Origin-Destination (O-D) travel demand matrixes while  
93 providing detailed traffic network configuration, which is commonly defined in terms of geometry, link capacities,  
94 free-flow speeds, and so on (Gomes et al., 2004). Moreover, the dynamic model can simulate each vehicle's  
95 instantaneous running activities, including acceleration and deceleration operations. INTEGRATION (Rakha et  
96 al., 2004), TRANSIMS (Zietsman et al., 2001), and VISSIM (PTV 2005) are the three major representative  
97 integrated models. However, modeling applicability is the biggest issue for these models since there are huge  
98 traffic characteristic differences among different nations and areas. Some researches (Min et al., 2008) have  
99 argued that current existing traffic simulation models are not suitable for simulating actual transportation

100 conditions, especially the mixed traffic in the downtown area in China.

101 Additionally, these main models have seldom been applied to characterize spatial and temporal  
102 distribution and variation of traffic-related CO<sub>2</sub> emissions (Gregg et al., 2008). In most cases, estimating the total  
103 quantity of the emissions is the main objective of these models and attracts tremendous attention. However,  
104 research on the characteristics of spatiotemporal distribution and variation of traffic-related CO<sub>2</sub> emissions could  
105 provide the ability to understand the impact of traffic load and variations on CO<sub>2</sub> emissions volume and prioritize  
106 emission control and reduction strategies based on location.

107 At present, with the development of intelligent transportation systems (ITS) in many urban areas, large  
108 quantities and varieties of real-time traffic data collected by inductive loop, video, radar, infrared ray, and floating  
109 cars have been obtained (Zhang et al., 2007). It becomes possible to obtain the real-time transportation conditions  
110 over the whole urban area from these data. In this paper, we present an integrated model to support area wide  
111 real-time transportation CO<sub>2</sub> emissions estimation. This study provides a framework for closely integrating the  
112 ITS technologies, GIS technologies and IVE models for GHG emission estimation. Within the framework, ITS  
113 technologies are applied to collect large-area real-time traffic data and generate the needed vehicle driving  
114 activities profiles. GIS technologies act as a database exchanger to organize all geographic-related information.  
115 The GIS toolset is also used to calculate CO<sub>2</sub> emissions in road-segment, and express the spatiotemporal  
116 distribution of the transportation CO<sub>2</sub> emissions in the urban area. The IVE model is imported to provide  
117 microscopic vehicle CO<sub>2</sub> emission rates. This paper is organized as follows. Section 2 introduces our approach on  
118 how to develop the integrated model. Section 3 describes our data preparation efforts. Section 4 analyzes our case  
119 study by using the ROSE model estimating the highway transportation GHG emissions in Beijing, China, in Dec.  
120 2008. Conclusions are presented in Section 5.

121

## 122 **2 MODEL DESCRIPTIONS**

### 123 **2.1 Framework of the ROad SEgment based Transportation CO<sub>2</sub> Emission Model**

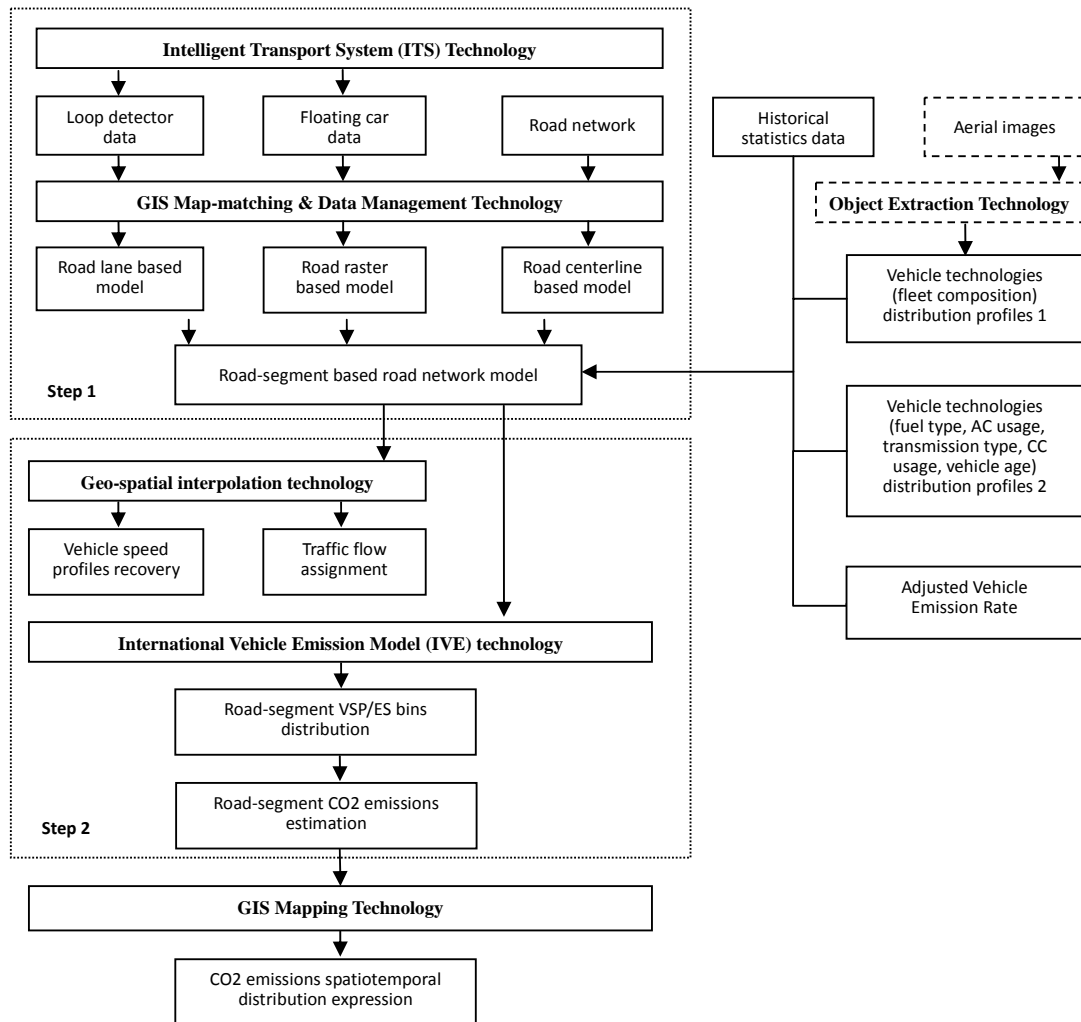
124 ROSE is an integrated model that seeks to carry out a combination of ITS technologies, GIS technologies and IVE  
125 models. ROSE facilitates the modeling of transportation CO<sub>2</sub> emissions production through integration of two  
126 main inter-linked steps. These are: 1) ITS real-time traffic data collection and geographic-related data unified  
127 organization; and 2) vehicle driving activities generation and urban area transportation CO<sub>2</sub> emissions  
128 computation.

129 The first step is to utilize GIS technologies to effectively organize and manage the ITS collected real-time  
130 traffic data such as floating car data (FCD), loop detector data (LDD), other geographic-related data (e.g., urban  
131 road network, digital elevation model (DEM), and aerial images) and statistical data (e.g., urban vehicle  
132 technologies distribution information). All these data will be given geographic coordinate information for  
133 identification and location. A three-level hierarchical structure (road centerline level-road segment level-road lane  
134 and road raster level) is specially designed for uniformly organizing these different types of data from the aspect of  
135 the spatial structure.

136 The second step is to utilize the IVE model to generate vehicle patterns, and vehicle specific power/engine  
137 stress bins distribution profiles from the well organized sampled real-time traffic data. Since these profiles could  
138 be resolved to each road segment, vehicle CO<sub>2</sub> emissions could be estimated in road segment partitions.

139 The final step is to take the ROSE model and apply it for estimation and analysis of the temporal and spatial  
140 distribution and variation of urban area transportation CO<sub>2</sub> emissions. GIS visualization tools can be used for CO<sub>2</sub>  
141 emissions expression.

142 The structure of ROSE is presented in FIGURE 1 and described in detail in the following sections.



143

144

**FIGURE 1 Main Framework of the ROAD SEGMENT Based Transportation CO<sub>2</sub> Emission Model.**

145

## 146 2.2 The Structure of ITS Real-time Traffic Data

147

148

149

150

151

152

153

154

155

156

157

158

159

160

In recent years, the floating-car system and fixed embedded loop detectors have been used as a way to collect transportation information in many nations and regions across the world. The data collection styles of floating cars and loop detectors are different - the former is mobile, while the latter is fixed. Furthermore, there are great differences in the aspects of recorded content and sampling time frequency. The probe data is recognized as a tool to describe the instantaneous vehicle activities, while the loop detector is suitable to record the traffic flow, occupancy, and average speed on a lane scale during a fixed time period. The sampling time interval (e.g., 1 s, 10 s, 30 s, 40s, 60s or more) of GPS data is mainly determined by subjective experiences for different applications. For the loop detectors, the sampling time intervals are generally fixed (e.g., 30 s, 60 s, 120s or more). Thus, when organizing and applying these heterogeneous traffic data, there is a need to unify traffic data from the perspectives of both spatial and temporal structure.

Based on the Map Matching Algorithm (Quddus et al., 2003), the floating car data and the loop detector data with the geographic information (e.g., longitude, latitude, and height) can be projected and matched with the road network and each data will be correlated with only one road unit. Since the traffic conditions in different road sections are different, we divide the road network into a great deal of road segments of suitable length. Each road

161 segment is considered as one road block holding the floating car and loop detector datasets. From the outside road  
 162 segment, both data are unified with the same spatial structure. Each dataset depicts the traffic conditions of the  
 163 corresponding road segment. The inside structures of both data also need to be well organized. Details are  
 164 described in the following sections. Because the sampling frequency of the loop detectors is lower than the  
 165 sampling frequency of the floating cars, the fixed sampling time interval of the loop detectors will be chosen to be  
 166 the basic time unit for data integration.

167

### 168 2.2.1 Horizontal Aggregation for Raster-Based Floating Car Data

169 The floating cars record the vehicular running status and the instantaneous position of the car. Frequently,  
 170 compared to the adjacent vehicles, one vehicle shows a similar moving pattern. One virtual point can be used to  
 171 represent the behaviors of the adjacent points in a relatively small section on the road. This section is defined as a  
 172 road raster and can be generated through the road network Rasterizing Algorithm. When there are more than one  
 173 floating car points matched into the same raster, the virtual point speed of the road raster is estimated by using the  
 174 Exponential Smoothing Method (Arroyo, 2007). The abstract form of the Exponential Smoothing Method is:

$$175 \quad \bar{V}_i(k) = F \left[ V_{i1}(k), V_{i2}(k), \dots, V_{ip}(k), V_{i1}(k-1), V_{i2}(k-1), \dots, V_{iq}(k-1) \right] \quad (1)$$

176 where  $\bar{V}_i(k)$  is the smooth average speed,  $V_{iw}(k)$  is the velocity of the  $w^{\text{th}}$  sampling floating car during time interval  
 177  $k$ ,  $p$  is the total number of the sampling points matched to the road raster  $i$  during time interval  $k$ , and  $q$  is the total  
 178 number of the sampling points matched to the road raster  $i$  during previous time interval  $k-1$ . The detailed equation  
 179 of  $\bar{V}_i(k)$  is as follows:

$$180 \quad \begin{aligned} \bar{V}_i(k) &= (1-f(k))\bar{V}_i(k-1) + f(k)\bar{V}_i(k) \\ f(k) &= r \cdot \left| \frac{E_k}{A_k} \right|, \bar{V}_i(k) = \frac{1}{n(k)} \cdot \sum_{j=1}^{n(k)} V_{ij}(k) \\ E_k &= r \cdot e_k + (1-r)E_{k-1}, A_k = r \cdot |e_k| + (1-r)A_{k-1} \\ e_k &= \bar{V}_i(k) - \bar{V}_i(k-1), r = \frac{n(k)}{1+n(k)} \end{aligned} \quad (2)$$

181 where  $\bar{V}_i(k)$  is the arithmetic average speed,  $f(k)$  is weighting coefficient,  $E_k$  is defined as the smooth error,  $A_k$   
 182 is defined as the smooth absolute error,  $e_k$  is defined as the error of estimation, and  $n(k)$  is the number of the  
 183 sampling floating car data points matched to raster  $i$  during time interval  $k$ .

184 In this method, each road raster is assigned a smooth average velocity during the time interval  $k$ . The adjacent  
 185 road raster will then be horizontally aggregated together as the road segment. The velocity dataset of the vehicles  
 186 in the road segment can be generated by a horizontally linear scan, represented by mathematic Equation 3:

$$187 \quad \bigcup_{i=1}^n \bar{V}_{[c,R_i]}^{t_j} = [\bar{V}_{[c,R_1]}^{t_j}, \bar{V}_{[c,R_2]}^{t_j}, \bar{V}_{[c,R_3]}^{t_j}, \dots, \bar{V}_{[c,R_n]}^{t_j}] \quad (3)$$

188 where  $n$  is the total count of the road raster of a road segment,  $R_i$  is the  $i^{\text{th}}$  road raster, and  $t_j$  is the time period. The  
 189 dataset can be processed to invert the speed fluctuation in the road during a given time period.

190

### 191 2.2.2 Vertical Aggregation for Lane Based Loop Detector Data

192 The loop detector data (LDD) reports the directional lane-by-lane value of the number of vehicles crossing the  
 193 lane in a given time period. These data, filtrated by the loop detector ID number and the traffic flow direction  
 194 identification, can be vertically aggregated as the dataset for each road segment:

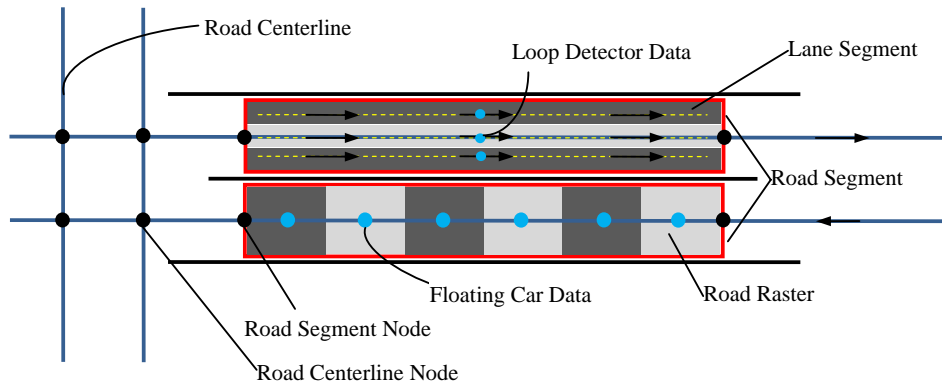
$$\bigcup_{l=1}^m F_{[c,L_i]}^{t_j} = [F_{[c,L_1]}^{t_j}, F_{[c,L_2]}^{t_j}, F_{[c,L_3]}^{t_j}, \dots, F_{[c,L_m]}^{t_j}] \quad (4)$$

where,  $m$  is the total lane number of each road segment,  $L_i$  is the  $i^{\text{th}}$  lane, and  $t_j$  is the time period. The dataset can be processed for computing the average road traffic flow.

197

### 2.2.3 Hierarchical Road Segment Based Road Network Model

In this paper, a hierarchical structure of the road network integrated with the real-time traffic data is proposed as shown in **FIGURE 2**.



202

203

**FIGURE 2 Hierarchical Structure of the Road Network.**

The characteristics of each hierarchical structure are illustrated as follows:

204

**Level 1: Road Centerline.** This provides an abstract structure of the road network by using a single line to depict the road and treats a cross or flyover as several links and nodes. Two road centerlines with different directions are aggregated into one whole street. The road is a collection of lanes with the same flow direction. The direction from or nearly from east to west or south to north is recorded as "0", otherwise is "1". The one-way street is also depicted as two road centerlines, but recorded as the same direction.

205

**Level 2: Road Segment.** Road segment is an area based structure with a certain width. The spatial structure and topology is derived from the road centerline based road network while the length is determined by the distribution of the loop detectors. Each road segment is a collection of the horizontally aggregated road raster and vertically aggregated lane segments. It is the basic unit for the CO<sub>2</sub> amount, and density computation and expression.

206

**Level 3: Lane Segment and Road Raster.** Both the lane segment and road raster are virtual structures of the road network. They are used for traffic data organization and management, CO<sub>2</sub> amount and density computation though they are not the basic unit for expression. Lane segment and road raster are the medium for correlating the road network with the real-time traffic data. Loop detector and floating car data series described in the above are recorded as the attributes of the lane segment and road raster, respectively.

207

**FIGURE 3** shows the process of integration of road network and real-time traffic data. First, the road network is converted from the structure of road centerline to the structure of the road segment which is aggregated by the lane segments and road raster. Each road raster and lane segment is then mapped with the real-time floating car data and loop detector data, respectively.

208

209

210

211

212

213

214

215

216

217

218

219

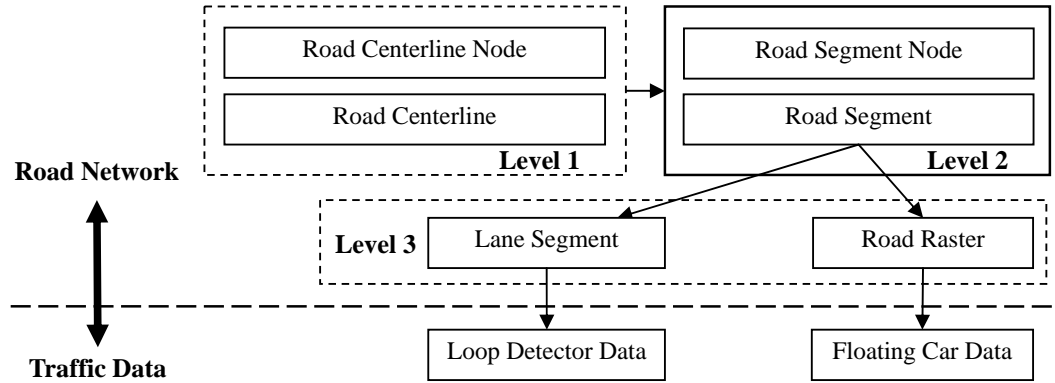
220

221

222

223

224



225  
226 **FIGURE 3 Process of Integration of Road Network and Real-time Traffic Data.**  
227

## 228 2.3 Emissions Estimation

### 230 2.3.1 Overview of IVE Model Technology

231 Compared to other familiar vehicle emission models, the IVE model (Davis et al., 2005) adopts binning  
232 methodology to describe and characterize driving patterns. The binning methodology is based on two parameters:  
233 vehicle specific power (VSP), and engine stress (ES). These two parameters indicate the relationship between the  
234 vehicle's instantaneous working condition and the emission rate. VSP is the main indicator of vehicle based  
235 emissions rate, which comprehensively considers most key factors (e.g., vehicle instantaneous speed and  
236 acceleration, road grade, road slope, wind, etc.) that influence the vehicle emission amount. The VSP equation is:

$$237 \quad VSP = 132 * v + 302 * v^2 + 1.1 * 10^6 * v * a + 9.81 * \text{Atan}(\text{Sin}(\text{Grade})) \quad (5)$$

238 where  $v$  is the vehicle instantaneous speed (m/s),  $a$  is the vehicle instantaneous acceleration (m/s<sup>2</sup>), and  $grade$  is  
239 the road grade in radians.

240 Vehicle stress (STR) uses an estimate of vehicle RPM combined with the average of the power exerted by the  
241 vehicle in the 15 seconds before the event of interest. The STR equation is:

$$242 \quad STR = RPM + 0.08 * \text{PreaveragePower} \quad (6)$$

243 Except the environment factors, VSP and STR values can be easily calculated from second-by-second  
244 vehicle route points. The VSP and STR values are broken into 20 VSP bins and 3 STR bins. In total, each point  
245 can be allocated into one of the 60 driving bins. For each type of vehicle technology, there are 60 adjusted  
246 emission rates corresponding to 60 bins.

247 To present a city's emission inventory, one important step is to present the distributions of driving activities  
248 that occur in each driving bin.

### 249 2.3.1 Road-segment Fleet Driving Activities Generation

250 It is obvious that using 1-Hz GPS data is adequate for describing the high-resolution driving activities of the  
251 vehicles including the immediate acceleration or deceleration. Such sampling frequency can provide enough  
252 sensitivity to detect the micro change of the vehicle's velocity. However, completely collecting the high-precision  
253 data set covers the entire urban area and is difficult and very time consuming. One solution is to use the  
254 interpolation method to revert the large area-covered but relatively low-frequency sampling FCD into the  
255 vehicle's real continuous running activities. The fundamental idea of cubic spline interpolation is based on the

256 engineer's tool used to draw smooth curves through a number of points. The numerical routine is to fit  $n$  equations  
 257 subject into the boundary conditions of  $n+1$  data points over  $n$  intervals. Cubic spline interpolation method must  
 258 satisfy three conditions as follows:

- 259 1.  $\hat{V}(x)$  will be continuous on the interval  $[x_1, x_n]$ ;
- 260 2.  $\hat{V}(x)$  is differentiable, and  $\hat{V}'(x)$  will be continuous on the interval  $[x_1, x_n]$ ;
- 261 3.  $\hat{V}(x)$  is also twice differentiable, and  $\hat{V}''(x)$  will be continuous on the interval  $[x_1, x_n]$ .

262 The assumed form for curve fit for each segment is defined as a separate third degree polynomial  $\hat{v}_i$ , which  
 263 is defined by

$$264 \quad \hat{v}_i(x) = a(x - x_i)^3 + b(x - x_i)^2 + c(x - x_i) + d_i \quad (7)$$

for  $i = 1, 2, \dots, n$

265 where the spacing between the successive data points is  $h_i = x_i - x_{i-1}$

266 To make the curve pleasingly smooth across the interval, the function value, the 1<sup>st</sup> derivative, and the 2<sup>nd</sup>  
 267 derivative must be equal at the interior node points for adjacent segments; that is,

$$268 \quad \left. \begin{aligned} \hat{v}(x_i - 0) &= \hat{v}(x_i + 0) \\ \hat{v}'(x_i - 0) &= \hat{v}'(x_i + 0) \\ \hat{v}''(x_i - 0) &= \hat{v}''(x_i + 0) \end{aligned} \right\} \text{for } i = 1, 2, \dots, n-1 \quad (8)$$

269 Define  $s''(x_i) = M_i$  (for  $i = 0, 1, 2, \dots, n$ ), where  $M_i$  is a one degree polynomial, for the  $i^{\text{th}}$  segment, the governing  
 270 equation is:

$$271 \quad h_i M_{i-1} + 2(h_i + h_{i+1})M_i + h_{i+1} M_{i+1} = 6(f[x_{i+1}, x_i] - f[x_i, x_{i-1}]) \quad (9)$$

for  $i = 1, 2, \dots, n-1$

272 where  $f[x_{i+1}, x_i]$  is the slope for the line across the start and end point of the  $i^{\text{th}}$  road segment;  $M_0$  and  $M_n$  are zero  
 273 for the natural spline boundary condition.

274 The fundamental idea underlying the cubic spline interpolation is to draw a smooth fleet speed  
 275 fluctuation curve through the virtual points aggregated in a road segment. The numerical routine is to fit  $n$   
 276 equations subjected to the boundary conditions of  $n + 1$  virtual points over the  $n$  road rasters. Based on the cubic  
 277 spline interpolation theory, once the dataset  $\bigcup_{i=1}^n \hat{V}_{[i, R]}$  is obtained, the continuous fleet speed fluctuation curve

278 between the road raster in a road segment scale can be fitted.

279

### 280 2.3.2 Road-segment Vehicle Kilometers Traveled (RS-VKT)

281 Vehicle miles traveled (VMT) or vehicle kilometers traveled (VKT) is commonly considered as a major factor in  
 282 determining the emission amount in urban areas. In many recent applications (Smit et al., 2008; Wang et al., 2009),  
 283 VKT is an uncertain factor since the origin-destination profiles are generated from the traffic assignment models.  
 284 However, for a road segment, based on the real-time loop detector data, VKT estimation results become accurate

285 because VKT is correlated to the traffic volume and the road segment length. In the last section, the traffic volume  
 286 of the road segment is described as a dataset of the flows  $\bigcup_{l=1}^m F_{[c,L_l]}^{t_j} = [F_{[c,L_1]}^{t_j}, F_{[c,L_2]}^{t_j}, F_{[c,L_3]}^{t_j}, \dots, F_{[c,L_m]}^{t_j}]$ . Accordingly, the VKT  
 287 for the road segment can be easily computed using Equation 10.

$$288 \quad VKT_{[c,t]} = Flow_{[c,t]} * Length_{[c]} = \sum_{l=1}^m F_{[c,L_l]}^{t_j} * Length_{[c]} \quad (10)$$

289

### 290 2.3.3 Road-segment CO<sub>2</sub> Emissions Estimation

291 Within the ROad-SEgment CO<sub>2</sub> Emissions Estimation (ROSE) model, the total emission amount is the summary  
 292 of each road segment's CO<sub>2</sub> emission volume generated by vehicles. The road segment is adopted to be the basic  
 293 computational unit in the ROSE model. As shown in Equation 11, based on the IVE model, the overall CO<sub>2</sub>  
 294 running emissions (in grams) for road segment  $c$  during specific time period  $t$  is quantified by multiplying the  
 295 comprehensive CO<sub>2</sub> emission rate by the distance traveled and by the ratio of the average velocity of the standard  
 296 driving cycle and the modeled cycle. The comprehensive emission rate is the adjusted emission rate multiplied by  
 297 the fraction of the travel and the amount of the driving pattern for each technology (ISSRC & UCR, 2008).

$$298 \quad E_{[c,t]}^{running} = \frac{\bar{V}_{FTP} * VKT}{\bar{V}_{specific[c,t]}} * Q_{[c,t]}^{comprehensive} \quad (11)$$

$$Q_{[c,t]}^{comprehensive} = \sum_{b=1}^{60} (f_{[c,t,b]} * Q_{[b]})$$

299 where,  $\bar{V}_{FTP}$  is the average velocity of the standard driving cycle (a constant (g/km)),  $\bar{V}_{specific[c,t]}$  is the average  
 300 velocity (g/km) of the total vehicle trips,  $VKT$  is the vehicle kilometers traveled,  $Q_{[c,t]}^{comprehensive}$  is the road segment  
 301 comprehensive emission rate for total vehicles,  $f_{[c,t,b]}$  is the fraction of travel by a specific technology  $b$ ,  $Q_{[b]}$  is the  
 302 adjusted emission rate for technology  $b$  for road segment  $c$  during time period  $t$ .

303

## 304 3. Data Preparation

305 In our experiments, we collected data from 390 fixed loop detectors buried under the Beijing highway lanes and  
 306 more than 20,000 GPS devices installed in taxis running on the roads of the Beijing city urban area in Dec. 2008.  
 307 These data were obtained from the transportation agency in Beijing and several taxi companies. The sampling  
 308 time intervals of loop detector data and floating car data were 120s and 40s, respectively. The average distance  
 309 between two adjacent loop detectors was less than one kilometer and the spatial distribution of the loop detector is  
 310 shown as green pin points in FIGURE 4. The city road network data is obtained from the company NavInfo,  
 311 China.

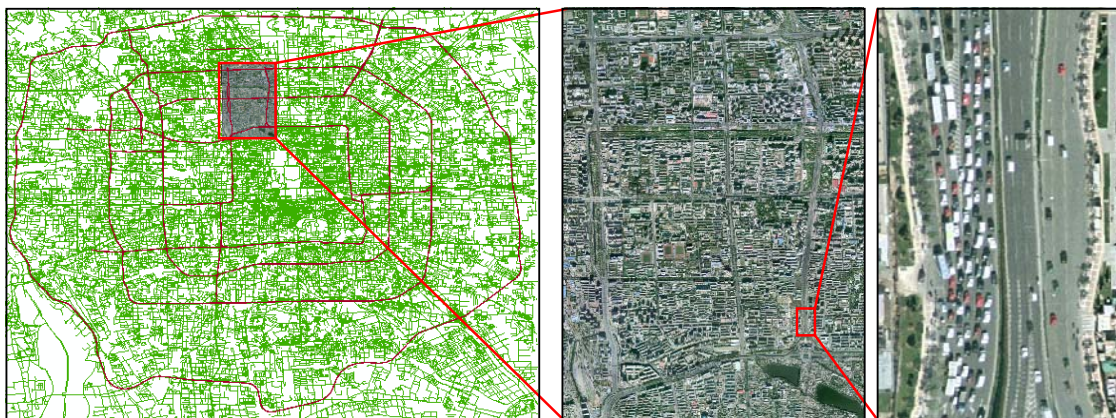


312

313 **FIGURE 4 Highway Network and Spatial Distribution of the 390 Loop Detectors Fixed in the Four Ring**  
 314 **Roads and Road Links within the Urban Area of Beijing City.**

315

316 Object extraction and detection technology (Hinz et al, 2001) and assistant manual judgment were applied to  
 317 generate the statistical Vehicle Class Distributions profile in Beijing from a high resolution aerial image  
 318 photographed in 2008. The image represents an area located in the Haidian District of about 19.4 square km  
 319 (3.15km\*6.16km) from the inner ring road to the outer ring road (FIGURE 5). The results show that the majority  
 320 of the vehicles, more than 73.9%, were passenger cars. Other types of vehicles in the fleet composition include  
 321 taxis (19.6%), buses (4.8%), and trucks (1.7%), etc.



322

323

324 **FIGURE 5 Photographed Area located in Haidian District, Beijing, China (2008).**

325

326 Other key statistical data about the Beijing vehicle technologies distribution (e.g., fuel type, air conditioning  
 327 system usage, transmission type, vehicle age, catalytic converter) and adjusted vehicle emission rates, were  
 328 imported from the report on Beijing Vehicle Activity Study (Liu et al, 2005) and the IVE official website  
 329 <http://www.issrc.org/ive/>. These data were used for measuring the comprehensive road segment emission rate in  
 this study.

330

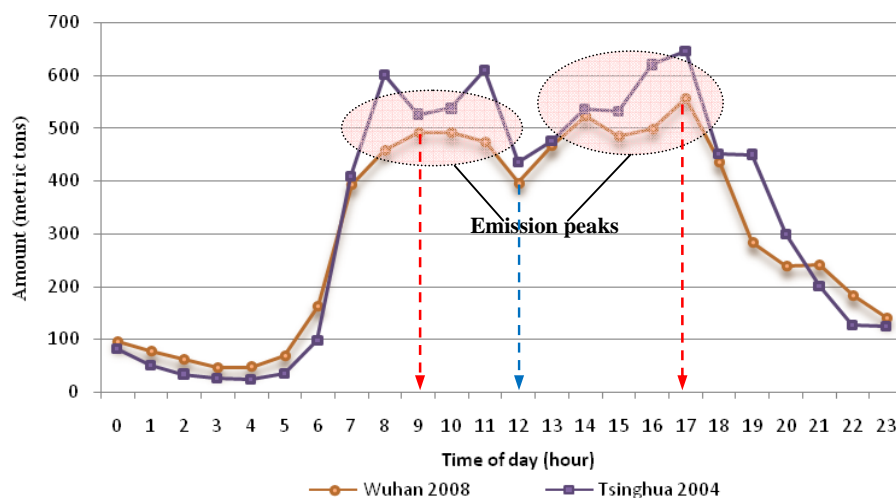
331 **4. CASE STUDY**332 **4.1 Study Area and Time**

333 The urban highway transportation system of Beijing city was chosen as our study subject. The Beijing highway  
 334 system within the urban area includes four ring roads (loop highways) and multiple links between ring roads. The  
 335 total length of the highways in our study is about 310 kilometers. Our experiment modeled the CO<sub>2</sub> emission on  
 336 Dec. 9, 2008 when the Olympics and Paralympics had been closed about three months. We used the ROSE model  
 337 to demonstrate the daily CO<sub>2</sub> emissions from the Beijing highway transportation in 2008 based on real-time traffic  
 338 data.

339

340 **4.2 Experiment Results**

341 According to our experiments, on Dec. 9, 2008, the total CO<sub>2</sub> emissions emitted from vehicles that passed through  
 342 the Beijing highway system was approximately 7,341 tons. The detailed hourly variation of the aggregated CO<sub>2</sub>  
 343 emissions from the highway within Beijing is shown in FIGURE 6. There are two obvious CO<sub>2</sub> emission peaks in  
 344 the diurnal time and one clear trough in nocturnal time. The peak CO<sub>2</sub> emission occurred around 9:00 and 17:00,  
 345 in the range of 500 tons and 550 tons per hour, respectively. These two time periods were chosen because they are  
 346 the rush hour for people going to work and coming back home. Between these two peaks, there is one small trough  
 347 around 12:00am, as it is lunch time. The hourly CO<sub>2</sub> emission amount increased rapidly from 6:00 to 7:00, while it  
 348 declined quickly from 18:00 to 19:00. The lowest hourly emission rate was about 45 tons per hour which occurred  
 349 around 3:00am in the early morning. Obviously, between 10:00pm in the evening and 7:00am in the morning, the  
 350 hourly CO<sub>2</sub> emission rate was very low and far less than 200 tons. Disaggregating total emissions according to the  
 351 time of day revealed that: 11.6% were at the AM peak time (7:00-9:00), 52.2% at the inter-peak time (9:00-17:00),  
 352 13.6% during the PM peak time (17:00-19:00), and 22.6% in the evening, night time, and the early morning  
 353 (19:00-7:00).



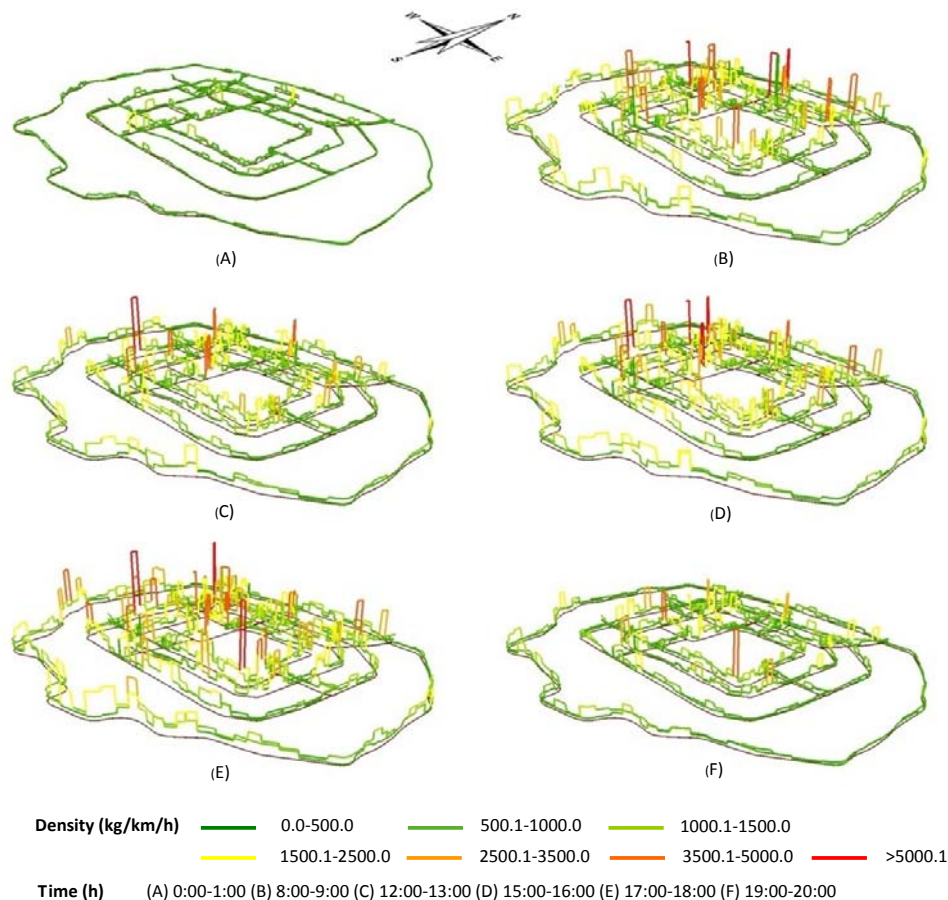
354

355 **FIGURE 6 Comparison of the Results of Hourly Variation of CO<sub>2</sub> Emissions for Beijing Highway**  
 356 **Estimated by Tsinghua University's Approach and ROSE, Respectively.**

357

358 The spatial-temporal distribution of the CO<sub>2</sub> highway emission rate in Beijing is revealed in FIGURE 7.  
 359 Six representative time periods, such as rush hour, work hour, and so on, were chosen to depict the spatial

360 distribution and variation of the CO<sub>2</sub> emission linear density. The CO<sub>2</sub> emission linear density is defined as the  
 361 weight (in kilograms) of CO<sub>2</sub> emissions per kilometer per hour (kg/km/h). It was concluded that the CO<sub>2</sub> densities  
 362 changed at different times and areas. During the night time, the CO<sub>2</sub> emissions level of most of the roads was far  
 363 less than 500 kilograms per kilometer per hour while during the PM peak time, the CO<sub>2</sub> emissions linear density of  
 364 many road segments reached 3500 kilograms per kilometer per hour or even more. Some road segments reached  
 365 as high as 5000 kilograms per kilometer per hour during rush hour. FIGURE 7 shows the spatial distribution  
 366 nonuniformity of CO<sub>2</sub> emissions and depicts some inherent laws as well. Our experiment results also demonstrate  
 367 that there was a trend that the hourly CO<sub>2</sub> emission density increased from the outer ring roads to inner ring roads  
 368 and from north-west to south-east.



373 **FIGURE 7 Representative Spatiotemporal Distribution of Road Segment CO<sub>2</sub> Emissions Linear Density**  
 374 **(kg/km/h) for Beijing Highway Network on Dec. 9, 2008 Estimated by ROSE.**

### 376 4.3 Discussion

377 As shown in FIGURE 6, the fluctuation and variation of the amount of highway CO<sub>2</sub> emissions shows a similar  
 378 change pattern in the results developed by both Tsinghua University (Liu et al, 2005) and our ROSE model.  
 379 Compared to the results from Tsinghua University's study, the CO<sub>2</sub> emissions hourly fluctuation curve developed  
 380 by our approach is more smooth and close to reality. Our approach decreased the uncertainties, especially those  
 381 that happened in the evening and night, while the video-based investigation approach has difficulty getting real  
 382 time traffic data. Additionally, the real-time traffic data based approach is sensitive enough to reveal everyday's  
 383 CO<sub>2</sub> emissions variation while the statistical approach is relatively static.

384 One interesting phenomenon found is that during the peak CO<sub>2</sub> hours, the total amount of CO<sub>2</sub> emissions  
385 in 2008 was lower than the total amount in 2004 in Beijing. It was mainly because of the local government urban  
386 traffic restriction rules. In 2008, Beijing's authority issued a novel and special traffic control rule named  
387 "odd-even" traffic restrictions for reducing the daily vehicle numbers traveled in the urban area. The rule had been  
388 enforced several months before the Olympic Games. This rule limited the particular number of vehicles traveling  
389 on the road. Cars were only allowed to travel in the Beijing urban area on alternate days depending on whether  
390 their license plate numbers ending in particular numbers. The restrictions divided vehicles into five groups. For  
391 example, cars with plate number ended in "0" or "5" were not allowed to drive on road on Monday; cars with the  
392 number of "1" or "6" at the end of their license plate were not allowed to travel in the urban area on Tuesday. In the  
393 same way, the remaining cars with specific numbers were not allowed to drive on the corresponding workday.  
394 Saturday and Sunday were free from the above restrictions. When the 2008 Beijing Olympic games ended, these  
395 special restrictions continued to be enforced. As is shown in FIGURE 7, our results have shown that these traffic  
396 restriction rules received great success in reducing vehicles generating GHG. There is approximately 20% daily  
397 reduction of the vehicle generated CO<sub>2</sub> emissions in the Beijing urban area.  
398

## 399 **5. CONCLUSION**

400 This paper presents an approach to estimate the total, spatiotemporal distribution and variation of urban area  
401 traffic CO<sub>2</sub> emissions based on various real-time traffic data (e.g., floating car data, loop detector data).  
402 Furthermore, this paper provides a framework of the ROad SEgment-based Transportation CO<sub>2</sub> Emission Model  
403 (ROSE) that integrates the road network, real-time traffic data, and the IVE model. The ROSE model was applied  
404 to the highways of Beijing city on Dec. 9, 2008. The overall traffic-related CO<sub>2</sub> emission was computed and the  
405 daily variation patterns were analyzed. Current work has demonstrated that the ROSE model is a useful tool for  
406 accurately estimating the traffic-related greenhouse gas emissions. An important finding is that some traffic  
407 restriction rules can greatly reduce the urban transportation GHG emissions.

408 Several areas of research are recommended to expand the applicability and scope of the ROSE model.  
409 First, CO<sub>2</sub> emission model/approach for the urban area without adequate real-time traffic data need to be  
410 developed. Second, real-time traffic data input standards, including the data structure and the attribute format need  
411 to be built up. Third, approaches for integrating the micro-scopic transportation simulation model need to be  
412 considered. To create a "low-carbon" society, further work will be focused on the traffic conditions, especially the  
413 impact traffic congestion has on the traffic related GHG emissions. Correspondingly, traffic restrictions and rules  
414 that influence the traffic conditions also need to be effectively assessed.  
415

## 416 **Acknowledgements**

417 Work described in this paper was jointly supported by key projects from National Science Foundation of China  
418 NSFC (No. 40830530) and NSFC project (No. 60872132). This paper has been partially authored by employees of  
419 UT-Battelle, LLC, under contract DE-AC05-00OR22725 with the U.S. Department of Energy. Accordingly, the  
420 United States Government retains and the publisher, by accepting the article for publication, acknowledges that  
421 the United States Government retains a non-exclusive, paid-up, irrevocable, world-wide license to publish or  
422 reproduce the published form of this manuscript, or allow others to do so, for United States Government purposes.  
423

## 424 **Reference**

- 425 [1]. Abo-Qudais, S., & Abu Qdais, H. (2005). "Performance evaluation of vehicles emissions prediction  
426 models," *Clean Technologies and Environmental Policy*, vol. 7, pp. 279-284.
- 427 [2]. Arroyo, J., Muñoz San Roque, A., Maté, C., Sarabia, A., (2007). "Exponential smoothing methods for  
428 interval time series". *Proceedings of Symposium, Espoo (Finland)*, pp. 231-240.
- 429 [3]. Barth, M. & Boriboonsomsin, K. (2008). "Real-world carbon dioxide impacts of traffic congestion",  
430 *Transportation Research Record*, Vol. 2058, pp. 163-171.
- 431 [4]. Barth, M., An, F., Norbeck, J., and Ross, M. (1996). "Modal Emissions Modeling: A Physical Approach,"  
432 In *Transportation Research Record 1520*, TRB, National Research Council, Washington, D.C., pp. 81-88.
- 433 [5]. Borrego, C., Tchepel, O., Costa, A.M., Amorim, J.H., & Miranda, A.I. (2003). "Emission and dispersion  
434 modelling of Lisbon air quality at local scale," *Atmospheric Environment*, vol. 37, pp. 5197-5205.
- 435 [6]. Carmichael GR, Sandu A, Chai T, Daescu DN, Constantinescu EM, Tang Y. (2008). "Predicting air  
436 quality: improvements through advanced methods to integrate models and measurements," *comput  
437 phys*, vol. 227, pp.3540-71.
- 438 [7]. Davis N, Lents J, Osses M, Nikkila N, Barth M. (2005). "Development and application of an  
439 international vehicle emissions model," *Transportation Research Board 81st Annual Meeting*, Washington  
440 D.C.
- 441 [8]. Escobedo FJ, Wagner JE, Nowak DJ, De la Maza CL, Rodriguez M, Crane DE. (2008). "Analyzing the  
442 cost effectiveness of Santiago, Chile's policy of using urban forests to improve air quality," *J Environ  
443 Manag*, vol. 86, pp.148-57.
- 444 [9]. Gomes, G., May, A.D., Horowitz, R. (2004). "Congested freeway microsimulation model using Vissim,"  
445 *Transportation Research Record: Journal of the Transportation Research Board*, vol. 1876, pp. 71-81.
- 446 [10]. Gregg, J., & Andres, R. (2008). "A method for estimating the temporal and spatial patterns of carbon  
447 dioxide emissions from national fossil-fuel consumption," *Tellus, B*, 60, pp. 1-10.
- 448 [11]. Intergovernmental Panel on Climate Change (IPCC) (2007) "Climate Change 2007: Impacts, Adaptation,  
449 and Vulnerability," Fourth assessment report.
- 450 [12]. ISSRC & UCR. (2008). Development of the Base Emission Rates for Use in the IVE Model Version 1.2,  
451 see <http://www.issrc.org/ive/> accessed Jan 2010.
- 452 [13]. Lents J, Davis N, Nikkila N, Osses M. (2004) "São Paulo vehicle activity study", Available online at  
453 <http://www.issrc.org/ive/>, International Vehicle Emissions Model.
- 454 [14]. Liu Huan, He Chunyu, James Lents, et al. (2005) "Beijing Vehicle Activity Study", Available online at  
455 <http://www.issrc.org/ive/>, International Vehicle Emissions Model.
- 456 [15]. Liu, H., He, K., Wang, Q., Huo, H. & Lents, J. (2007). "Comparison of Vehicle Activity and Emission  
457 Inventory between Beijing and Shanghai," *Journal of the Air & Waste Management Association*, vol. 57, pp.  
458 1172-1177.
- 459 [16]. Min G, Du Y M, Wu J P, & Yan S. (2008). "Simulation Study of Mixed Traffic in China--a Practice in  
460 Beijing," *Proceedings of the 11th International IEEE Conference on Intelligent Transportation Systems* Beijing,  
461 China, October 12-15, pp. 281-285.
- 462 [17]. Davis, Nicole, James Lents, Nick Nikkila, et al. (2004) "Mexico City Vehicle Activity Study", Available  
463 online at <http://www.issrc.org/ive/>, International Vehicle Emissions Model.
- 464 [18]. PTV Planung Transport Verkehr AG (2005). VISSIM 4.10 User Manual. Germany.
- 465 [19]. Quddus, M. A., W. Y. Ochieng, L. Zhao, & R. B. Noland. (2003) "A General Map Matching Algorithm  
466 for Transport Telematics Applications". *GPS Solutions*, Vol. 7, pp. 157-167.
- 467 [20]. Smit, R., M. Poelman and J. Schrijver. (2008) "Improved road traffic emission inventories by adding  
468 mean speed distributions", *Atmos Environ* Vol. 42, pp. 916-926.

- 469 [21]. Rakha, H., & Ahn, K. (2004). "INTEGRATION Modeling Framework for Estimating Mobile Source  
470 Emissions," *Journal of Transportation Engineering*, vol. 130, pp. 183-193.
- 471 [22]. Rakha, H., Ahn, K., & Trani, A. (2003). "Comparison of MOBILE5a, MOBILE6, VT-MICRO, and CMEM  
472 models for estimating hot-stabilized light-duty gasoline vehicle emissions," *Canadian Journal of Civil  
473 Engineering*, vol. 30, pp. 1010-1021.
- 474 [23]. Ribeiro, S. K., Kobayashi, S., Beuthe, M., Gasca, J., Greene, D., Lee, D., Muromachi, Y., Newton, P.,  
475 Plotkin, S., Sperling, D., Wit, R. & Zhou, P. (2007). "Transport and its infrastructure," in *climate change  
476 2007: Mitigation. Contribution of Working Group III to the Fourth Assessment Report of the Intergovernmental  
477 Panel on Climate Change*, Cambridge University Press, Cambridge, United Kingdom and New York, NY,  
478 USA.
- 479 [24]. Sharma, P., & Khare, M. (2001). "Modeling of vehicular exhausts - a review," *Transportation Research  
480 Part D6*. pp. 179-198.
- 481 [25]. Hinz, Stefan, and Albert Baumgartner. (2001) "Vehicle detection in aerial images using generic features,  
482 grouping, and context", *Lecture Notes on Computer Science*, pp. 45-52.
- 483 [26]. Wang H K, Chen C H, Huang C et al. (2006). "Application of the International Vehicle Emission model  
484 for estimating of vehicle emissions in Shanghai," *Acta Scientiae Circumstantiae*, vol. 26, pp. 1-9.
- 485 [27]. Wang, H., Fu, L., Lin, X., Zhou, Y., and Chen, J.( 2009): "A bottom-up methodology to estimate vehicle  
486 emissions for the Beijing urban area", *Science of the Total Environment.*, Vol. 407, pp. 1947-1953.
- 487 [28]. Zhang, C., Yang, X., Yan, X. (2007). "Methods for Floating Car Sampling Period Optimization," *Journal  
488 of Transportation Systems Engineering and Information Technology*, Vol.7, pp.100-104.
- 489 [29]. Zietsman, J., & Rilett, L. R. (2001). "Analysis of Aggregation Bias in Vehicular Emission Estimation  
490 using TRANSIMS Output," *Transportation Research Record: Journal of the Transportation Research Board*,  
491 vol. 1750, pp. 56-63.
- 492